ANIMAL LOCOMOTION

Vibrational control: A hidden stabilization mechanism in insect flight

Haithem E. Taha[1]*, Mohammadali Kiani[1], Tyson L. Hedrick[2], Jeremy S. M. Greeter[2,3]

It is generally accepted among biology and engineering communities that insects are unstable at hover. However, existing approaches that rely on direct averaging do not fully capture the dynamical features and stability characteristics of insect flight. Here, we reveal a passive stabilization mechanism that insects exploit through their natural wing oscillations: vibrational stabilization. This stabilization technique cannot be captured using the averaging approach commonly used in literature. In contrast, it is elucidated using a special type of calculus: the chronological calculus. Our result is supported through experiments on a real hawkmoth subjected to pitch disturbance from hovering. This finding could be particularly useful to biologists because the vibrational stabilization mechanism may also be exploited by many other creatures. Moreover, our results may inspire more optimal designs for bio-inspired flying robots by relaxing the feedback control requirements of flight.

INTRODUCTION

Insect flight was deemed impossible for decades [e.g., (*1*–*4*)] because the required lift coefficients for balance are two to three times the maximum lift coefficients achieved by conventional aerodynamics. Then, biologists and engineers unraveled some of the unconventional lift mechanisms exploited by insect and bird flight. For example, a stabilized leading edge vortex, first introduced by Ellington and coworkers (*5*) and further explored by Dickinson *et al.* (*6*), forms the main unconventional lift mechanism that makes insect flight possible.

Seminal efforts by Ellington *et al.* (*5*) and Dickinson *et al.* (*6*), which unraveled the unconventional aerodynamic mechanisms of insect flight, have spawned research on the dynamics of flapping flight (*7*–*15*), the majority of which suggest that insects are unstable in hovering flight. The critical instability characteristics of the hovering equilibrium are manifested in the longitudinal plane $x - z$, as shown in Fig. 1. In this plane, the body has three degrees of freedom: translations along the x and z axes with velocity components u and w, respectively, and a rotation about the y axis (out of the page) represented by an angle θ and an angular velocity q. The forces X and Z are the aerodynamic forces in the x and z directions, respectively, and M is the aerodynamic pitching moment about the y axis.

Ignoring the wing structural and inertial effects, the longitudinal equations of motion are exactly the same as conventional aircraft (*16*)

$$\begin{pmatrix} \dot{u} \\ \dot{w} \\ \dot{q} \\ \dot{\theta} \end{pmatrix} = \begin{pmatrix} -qw - g\sin\theta \\ qu + g\cos\theta \\ 0 \\ q \end{pmatrix} + \begin{pmatrix} X/m \\ Z/m \\ M/I_y \\ 0 \end{pmatrix} \quad (1)$$

where g is the gravitational acceleration, m is the body mass, and I_y is the body pitching inertia. However, unlike conventional aircraft, the aerodynamic loads X, Z, and M are time periodic, leading to a multi–time scale dynamical system: The relatively slow body flight dynamics is forced by the periodic aerodynamic loads due to the fast wing flapping oscillations. The ratio between these two time scales is deceptively large; for slow-flapping insects (e.g., *Manduca sexta*), the ratio between the flapping frequency and the flight dynamics natural frequency is around 30 (*10*, *17*), which naturally invokes averaging. That is, the aerodynamic loads oscillate with a frequency that is too high to affect the body, and thus, the body only responds to the mean values of the time-periodic aerodynamic loads.

Adopting direct averaging of Eq. 1, over the past two decades, the flapping flight dynamics community has reached a near consensus that insects are unstable at hover (*7*–*14*, *17*–*22*). For example, simplified modeling (shown in the Supplementary Materials) yields an averaged dynamics whose linearization about the hovering equilibrium is written as

$$\begin{pmatrix} \dot{\overline{u}} \\ \dot{\overline{w}} \\ \dot{\overline{q}} \\ \dot{\overline{\theta}} \end{pmatrix} = \begin{bmatrix} \overline{X}_u & 0 & 0 & -g \\ 0 & \overline{Z}_w & 0 & 0 \\ \overline{M}_u & 0 & \overline{M}_q & 0 \\ 0 & 0 & 1 & 0 \end{bmatrix} \begin{pmatrix} \overline{u} \\ \overline{w} \\ \overline{q} \\ \overline{\theta} \end{pmatrix} \quad (2)$$

where overbar indicates an averaged quantity and the terms X_u, Z_w, M_u, and M_q are aerodynamic stability derivatives. For example, X_u is the change in X force due to a u disturbance (i.e., damping in the forward direction) (*17*).

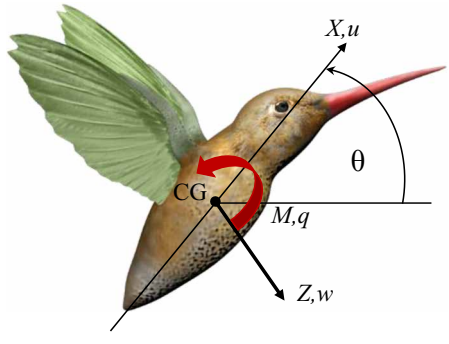

Fig. 1. Schematic of the longitudinal flight of a hovering animal. The variables u and w represent the body velocity components in the body frame, q is the pitch rate, and θ is the pitching angle. The forces X and Z are the aerodynamic forces in the body frame, and M is the aerodynamic pitching moment. [Hummingbird credit: Cartoomotion/cgtrader]

[1]Department of Mechanical and Aerospace Engineering, University of California, Irvine, Irvine, CA 92617, USA. [2]Department of Biology, University of North Carolina at Chapel Hill, Chapel Hill, NC 27599, USA. [3]Technology Deployment and Outreach, Pacific Northwest National Laboratory, Richland, WA 99352, USA.
*Corresponding author. Email: hetaha@uci.edu

The linear, time-invariant system Eq. 2 has the following eigenvalue structure for almost all insects: an unstable oscillatory mode (corresponding to a complex-conjugate pair of eigenvalues with a positive real part) and two stable non-oscillatory (aperiodic or subsidence) modes (corresponding to two negative real eigenvalues) (*9*–*14*, *17*, *19*, *22*). The unstable pair is mainly associated with pitching motion, implying that instability is primarily due to the lack of pitch stiffness, which can be seen in Eq. 2; there is no θ coefficient in the third row. That is, there is no restoring pitching moment (acceleration $\dot{q}$) proportional to a pitch disturbance θ (i.e., no pitch spring action or stiffness). In contrast, there is a substantial pitch damping M_q as seen in the q coefficient in the third row, which is referred to as flapping counter torque (*14*, *23*, *24*). These conclusions are well known to the flapping flight dynamics community.

The implication is that insects must use feedback control to stabilize their hovering flight (*8*, *25*–*27*). That is, an insect has to continuously monitor its attitude and provide stabilizing actions, which may necessitate considerable processing from the insect's brain whose computational capabilities are rudimentary: the insect's brain consists of about 3000 neurons (*28*), which is expressively described by Zbikowski (*29*) as "less computational power than a toaster." Nevertheless, pitch stability reflexes have been identified in many insects (*25*, *30*, *31*). However, it is less clear whether these reflexes are sufficient to stabilize the dynamics given by Eq. 2 during a full range of natural behavior.

The subtleties of averaging

Although the stability analysis (shown above) based on averaging is quite intuitive, it needs mathematical justification, which is provided by the averaging theorem: Consider the general form of a nonlinear, time-periodic system

$$\dot{\boldsymbol{\chi}} = \varepsilon \mathbf{F}(\boldsymbol{\chi}, t) \tag{3}$$

If $\mathbf{F}$ is T periodic in t, the averaged system corresponding to (3) is written as

$$\dot{\overline{\boldsymbol{\chi}}} = \varepsilon \overline{\mathbf{F}}(\overline{\boldsymbol{\chi}}) \tag{4}$$

where $\overline{\mathbf{F}}(\boldsymbol{\chi}) = \frac{1}{T}\int_0^T \mathbf{F}(\boldsymbol{\chi}, \tau)\, d\tau$. According to the averaging theorem [see Khalil (*32*) for example], if ε is small enough, then exponential stability of an equilibrium point of the averaged system implies exponential stability of the corresponding periodic orbit of the original time-periodic system. Therefore, the averaging theorem allows deducing stability of a time-varying system (Eq. 3) by studying the stability of a much simpler (time-invariant) system where there are plenty of analysis tools. Typically, ε is scaled with the reciprocal of the forcing frequency ω. That is, for high enough ω, stability of the averaged dynamics implies stability of the time-periodic dynamics.

The above discussion implies that direct averaging is only valid for high enough flapping frequencies. Unfortunately, this frequency threshold is not known a priori; only its existence is guaranteed by the averaging theorem (*32*), which indicates a potentially flawed analysis when using direct averaging, as pointed out by Berg and Wickramasinghe (*33*). In other words, how high should the frequency be for direct averaging to work? There might not be a more expressive statement about the subtleties of averaging than that by Sanders *et al.* in their book on the topic (*34*): Averaging is too intuitive for scientists and engineers to scrutinize its mathematical details. However, it must be applied rigorously to avoid its obscure pitfalls.

RESULTS

Here, we show that the direct averaging approach does not have sufficient rigor for the rich dynamics of insect flight. As such, it obscures some exquisite stability characteristics of these fascinating species. To honor the 70th birthday of Lev Pontryagin, the founder of optimal control theory, his students Agrachev and Gamkrelidze developed a new calculus for time-varying dynamical systems: the chronological calculus (*35*). On the basis of these advanced mathematical tools, Sarychev (*36*) and Vela (*37*) developed higher-order averaging techniques for time-periodic systems. Sarychev (*36*) introduced the notion of complete averaging to denote the following averaged dynamics of the nonlinear, time-periodic system (Eq. 3)

$$\dot{\overline{\boldsymbol{\chi}}} = \varepsilon \overline{\mathbf{F}}(\overline{\boldsymbol{\chi}}) = \varepsilon \boldsymbol{\Lambda}_1(\overline{\boldsymbol{\chi}}) + \varepsilon^2 \boldsymbol{\Lambda}_2(\overline{\boldsymbol{\chi}}) + \varepsilon^3 \boldsymbol{\Lambda}_3(\overline{\boldsymbol{\chi}}) + \ldots \tag{5}$$

where (*38*)

$$\boldsymbol{\Lambda}_1(\boldsymbol{\chi}) = \frac{1}{T}\int_0^T \mathbf{F}(\boldsymbol{\chi}, t)\, dt$$

$$\boldsymbol{\Lambda}_2(\boldsymbol{\chi}) = \frac{1}{2T}\int_0^T \left[\int_0^T \mathbf{F}(\boldsymbol{\chi}, \sigma)\, d\sigma, \mathbf{F}(\boldsymbol{\chi}, t)\right] dt$$

$$\boldsymbol{\Lambda}_3(\boldsymbol{\chi}) = -\frac{T}{2}[\boldsymbol{\Lambda}_1(\boldsymbol{\chi}), \boldsymbol{\Lambda}_2(\boldsymbol{\chi})] + \frac{1}{3T}\int_0^T \left[\int_0^T \mathbf{F}(\boldsymbol{\chi}, \sigma)\, d\sigma, \left[\int_0^T \mathbf{F}(\boldsymbol{\chi}, \sigma)\, d\sigma, \mathbf{F}(\boldsymbol{\chi}, t)\right]\right] dt$$

where the Lie bracket between two vectors is defined as $[\mathbf{V}_1, \mathbf{V}_2] = \frac{\partial \mathbf{V}_2}{\partial \boldsymbol{\chi}}\mathbf{V}_1 - \frac{\partial \mathbf{V}_1}{\partial \boldsymbol{\chi}}\mathbf{V}_2$. In the complete averaged dynamics, shown in Eq. 5, the first term $\boldsymbol{\Lambda}_1$ is simply the direct averaging of the dynamics. Therefore, if ε is small enough such that the higher-order terms in ε are negligible, the classical averaging theorem is recovered. However, if ε is not small enough, one should include higher-order terms from the series (Eq. 5) in the averaged dynamics. The main strength of the series (Eq. 5) lies in the fact that, if it converges and the limit vector field $\overline{\mathbf{F}}$ has an exponentially stable equilibrium point, then the original, nonlinear, time-periodic system (Eq. 3) will have an exponentially stable periodic orbit irrespective of the value of ε. Therefore, there is no approximation, and this is why Sarychev called it complete averaging.

Vibrational stabilization

Applying these tools, we find that the entries of the system (Eq. 2) are modified, hence altering the stability characteristics of insect flight dynamics. For example, the linearized, first- and second-order averaged dynamics of the hawkmoth are given by

$$\frac{\partial \boldsymbol{\Lambda}_1}{\partial \boldsymbol{\chi}}(\mathbf{0}) = \begin{bmatrix} -3.59 & 0 & 0 & -9.81 \\ 0 & -3.30 & 0 & 0 \\ 39.95 & 0 & -7.92 & 0 \\ 0 & 0 & 1 & 0 \end{bmatrix}, \frac{\partial(\boldsymbol{\Lambda}_1 + \boldsymbol{\Lambda}_2)}{\partial \boldsymbol{\chi}}(\mathbf{0})$$

$$= \begin{bmatrix} -3.58 & 0 & 0 & -9.81 \\ 0 & -3.09 & 0 & 0 \\ 29.98 & 0 & -8.13 & -28.45 \\ -2.90 & 0 & 0.96 & 0 \end{bmatrix}$$

As a result, the eigenvalues of the averaged system matrix $\frac{\partial \overline{\mathbf{F}}}{\partial \chi}(\mathbf{0})$ are shifted from [0.19 ± 5.74*i*, −11.89, −3.30.] to [−0.66 ± 3.72*i*, −10.40, −3.09] when adding the second-order averaging contributions. We attribute this stabilization to the creation of the element (3, 4) which represents pitch stiffness [the essential feature of static stability of conventional aircraft (*16*)]. The original hovering flight dynamics of insects lack any direct pitch stiffness (*17*). However, this higher-order averaging analysis revealed an indirect and unconventional spring action (pitch-stiffness) mechanism $\ddot{\bar{q}} = \ddot{\bar{\theta}} = -k_\theta \bar{\theta}$. This phenomenon is known to the dynamics and control community as vibrational stabilization/control [e.g., Baillieul and Lehman (*39*), Sarychev (*36*), and Bullo (*40*)] or stabilization via parametric excitation [e.g., Nayfeh and Mook (*41*)].

Vibrational stabilization is an interesting phenomenon whose history goes back to 1908, when Stephenson (*42*) analyzed the dynamics of an inverted pendulum whose pivot is subjected to vertical oscillation. The unstable vertical equilibrium of the inverted pendulum gains a robust stability when the pivot oscillates with a sufficiently high frequency. The first full nonlinear analysis of this problem was carried out by Kapitza (*43*, *44*), and hence, the problem is named after him: the Kapitza pendulum. Reference (*45*) shows the vibrationally induced spring action on the Kapitza pendulum. Here, we show that the natural vibration of insect wings induces stabilizing actions to its flight dynamics in a way similar to the Kapitza pendulum.

Physics of vibrational stabilization in insect flight dynamics

Using chronological calculus, we derived an analytical expression for the vibrationally induced spring constant (stiffness) k_θ for insect flight dynamics as

$$k_\theta = \frac{g}{2T}\int_0^T \left[M_{V_x}(t)\, t - \int_0^t M_{V_x}(\tau)\, d\tau \right] dt \qquad (6)$$

where T is the flapping period and M_{Vx} is the pitching moment changes due to the body horizontal speed $V_x = u\cos\theta + w\sin\theta$. Equation 6 is quite revealing for the nature of the vibrationally induced stiffness: k_θ is simply related to gravity and the "variation" of M_{Vx} over the flapping cycle. That is, if M_{Vx} were constant like a conventional aircraft or a non-oscillatory flying system, k_θ would vanish. Similar to all stability derivatives in insect flight, M_{Vx} can be decomposed into a mean value $\overline{M}_{V_x} > 0$ (*14*, *17*) and a zero-mean oscillatory contribution ΔM_{Vx}. The latter is due to the oscillation of the moment arm between the wing center of pressure and the body center of gravity (CG): In some times, the wing is behind the CG, and in other times, the wing is ahead of the CG. The heuristic value of the proposed analysis is shown in the derived relation (6), which suggests studying in some detail the effect of this fast-varying component ΔM_{Vx} on the animal's recovery from pitch disturbances (i.e., how does it induce a pitch stiffness k_θ?).

When the body experiences a pitch up disturbance $\Delta\theta$, the lift force will pull it backward, similar to a helicopter. The effect of this disturbance on the speed V_x decays due to damping (e.g., X_u). However, these damping derivatives change on the fast time scale. For example, X_u is given in the Supplementary Materials as (*17*)

$$X_u = -4\frac{K_{11}}{m}|\varphi|\cos^2\varphi\sin^2\eta$$

where K_{11} is a constant that depends on the morphological parameters; η is the wing pitching angle, which is taken as piecewise constant in the current simulation; and φ is the flapping angle. If φ varies harmonically as $\varphi = \Phi\cos\omega t$, then the signal $|\varphi|\cos^2\varphi$ will oscillate with double the frequency, as shown in Fig. 2A. This behavior is intuitively expected because damping depends on the absolute value of the flapping speed whether the wing is moving in the downstroke or upstroke direction. Now, this oscillation in damping in the forward direction is inherited in the response of the forward speed. For example, if one considers the following simple differential equation $\dot{u} = X_u u$ with $X_u = \overline{X}_u + A\cos 2\omega t$, where $\overline{X}_u$ is a nonzero mean value of the damping derivative X_u (*14*, *17*), then the exact solution to an initial disturbance u_0 is given by $u(t) = u_0 e^{\overline{X}_u t + \frac{A}{2\omega}\sin 2\omega t}$, which can be approximated for large ω as

$$u(t) \simeq \underbrace{u_0 e^{\overline{X}_u t}}_{\text{Averaged Response}} + \underbrace{\frac{A}{2\omega} u_0 e^{\overline{X}_u t}\sin 2\omega t}_{\text{Oscillatory Response}}$$

which shows the oscillatory response at double the flapping frequency. That is, the body (on the average) would recover from the initial V_x disturbance, though with an oscillatory V_x component, as shown in Fig. 2B, which presents a simulation of the full time-varying dynamics (Eq. 1) to a 30° pitch disturbance from hovering using the hawkmoth morphological parameters. In conclusion, the V_x response can be decomposed as $V_x = \overline{V}_x + \Delta V_x$, where $\overline{V}_x$ is the slow behavior determined by the averaged dynamics (Eq. 2) and ΔV_x is a zero-mean fast-oscillatory component that is typically ignored by direct averaging.

The restoring moment $M_{V_x} V_x = (\overline{M}_{V_x} + \Delta M_{V_x})(\overline{V}_x + \Delta V_x)$ can be decomposed into an averaged contribution $\overline{M}_{V_x}\overline{V}_x$, which is captured in the averaged system (Eq. 2), and vibrational or oscillatory contributions $\overline{M}_{V_x}\Delta V_x$, $\Delta M_{V_x}\overline{V}_x$, and $\Delta M_{Vx}\Delta V_x$, which are typically ignored by direct averaging. In particular, we focus here on the term $\Delta M_{Vx}\Delta V_x$, which is due to the oscillatory components of both the stability derivative M_{Vx} (i.e., the system dynamics) and the body response V_x. This vibrational contribution will have a net effect only

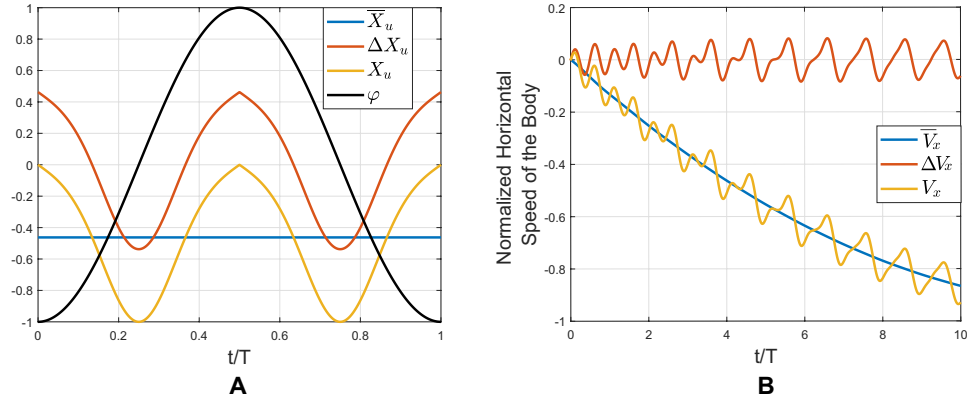

Fig. 2. Illustration of the oscillation in the forward damping X_u and forward speed V_x. (**A**) Variation of the normalized flapping angle φ and the (averaged and oscillatory) components of the normalized damping X_u in the forward direction, which is proportional to $|\varphi|\cos^2\varphi$. (**B**) Simulation of the nonlinear time-periodic system (see Eq. 1) to a 30° pitch disturbance from hovering using the hawkmoth morphological parameters. The body speed V_x is normalized by *R*/*T*, the flapping angle φ by the flapping amplitude, and the stability derivative X_u by its maximum value over the cycle.

if the two terms ΔM_{Vx} and ΔV_x have some synchronization (i.e., in-phase). For example, if they are 90° shifted (i.e., one signal is $\sin\omega t$ and the other is $\cos\omega t$), then their net effect over the cycle would vanish by virtue of the identity $\int_0^T \sin\omega t\cos\omega t = 0$.

The natural response of the body time-periodic dynamics (Eq. 1) results in ΔV_x that is synchronized with the wing motion and consequently ΔM_{Vx}, as shown by the simulation in Fig. 3A to a 30° pitch disturbance. We also zoom over the first cycle to show the synchronization between ΔM_{Vx} and ΔV_x so that their product is always negative. As such, it results in a restoring pitching moment that is proportional to the pitch disturbance, i.e., a spring action (V_x and ΔV_x are proportional to the θ disturbance). In other words, it is precisely the fact that M_{Vx} has a fast-varying component ΔM_{Vx}, due to the fast wing flapping oscillation, that leads to the stiffness k_θ when the body speed V_x changes due to pitch disturbance. This result is observed from Eq. 6, which results in zero k_θ if M_{Vx} is constant (i.e., replaced with its averaged value $\overline{M}_{V_x}$). Because ΔM_{Vx} is mainly due to the oscillatory wing motion, this synchronization is better presented between the oscillatory stroke position (or moment arm) and the oscillatory body speed ΔV_x, as shown in Fig. 3B, which sets the stage to explain the physics discussed above in Fig. 4.

Vibrational stabilization in a real hawkmoth experiment

To experimentally demonstrate the vibrational stabilization phenomenon in flapping flight dynamics, we analyzed the recovery of a real hovering hawkmoth from a pitch disturbance. For this experiment, hawkmoths (*M. sexta*) from a domestic colony were trained to fly in a glass-walled flight chamber and feed from an artificial nectar source. The moths were perturbed in pitch by striking them in mid-air with a projectile fired by a spring-loaded cannon as they approached the nectar source. We then used high-speed multicamera videography to measure the three-dimensional (3D) wing and body kinematics of the animal before and following impact (Fig. 5).

The objective is to demonstrate the physics underlying vibrational stabilization—namely, (i) the synchronization between the body horizontal speed and wing stroke and (ii) its vibrational contribution in the restoring moment $M_{Vx}V_x$ over the very first cycle after perturbation, which may represent a spontaneous response from the animal (perhaps with feedback control too) before departure. Three cases of hawkmoth perturbation from free hovering flight were considered: two pitch down perturbations and one pitch up. From the measured 3D kinematics of the wing and the body, we obtained the horizontal speed component V_x of the body CG and passed it to an eighth-order Butterworth filter (whose passband is between 1.5 and 2.5 the flapping frequency) to extract the fast-varying oscillatory component ΔV_x from the slowly varying one $\overline{V}_x$. We also obtained the longitudinal (along the body axis) component of the position vector between the wing tip and the body CG, which represents the wing stroke position or the moment arm. Then, a straightforward verification of the predicted synchronization between ΔV_x and the stroke position was directly performed from these kinematic measurements (no aerodynamic model was involved), as shown in Fig. 6 (A to C) for the three cases under study. These figures show a synchronization between ΔV_x and the stroke position in the real animal over the first cycle right after pitch perturbation that is quite similar to the predictions in Figs. 3 and 4, which lead to vibrational stabilization.

For a more quantitative analysis, we fed the measured 3D wing kinematics to an unsteady aerodynamic model (detailed in the Supplementary Materials) to determine an estimate for the stability derivative M_{Vx} over the cycle. This signal was decomposed into a cycle-averaged value $\overline{M}_{V_x}$ and a zero-mean oscillatory component ΔM_{Vx}. We then compared the averaged contribution $\overline{M}_{V_x}\overline{V}_x$ against

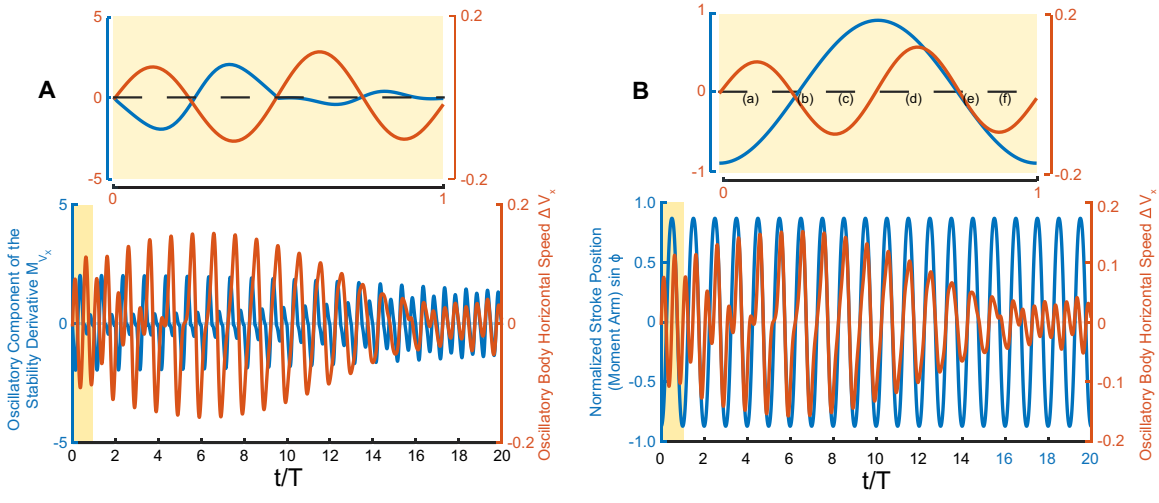

Fig. 3. Synchronization between the wing motion and body motion. Simulation of the nonlinear time-periodic system (see Eq. 1) to a 30° pitch disturbance from hovering using the hawkmoth morphological parameters. (**A**) Synchronization between the response of the oscillatory component ΔV_x of the body horizontal speed due to a pitch disturbance and the fast-varying component ΔM_{Vx} of the speed stability derivative M_{Vx}. Because ΔM_{Vx} is mainly due to the oscillatory wing motion, this synchronization is better presented between the stroke position and the oscillatory body speed component ΔV_x. (**B**) Synchronization between ΔV_x and the stroke position represented by the moment arm from the wing tip quarter-chord point to the body CG. The plots are normalized: the body speed V_x by R/T, the stroke position by R, and the stability derivative M_{Vx} by $1/(RT)$. ΔM_{Vx} is given by the adopted flight dynamic model (shown in the Supplementary Materials), whereas ΔV_x is obtained from the simulation of the time-periodic dynamical system (see Eq. 1) after applying a high-pass filter to extract the fast-varying component of the body speed V_x. Labels (a) to (f) at specific time instants during the cycle help elucidate the physics of vibrational stabilization in insect flight.

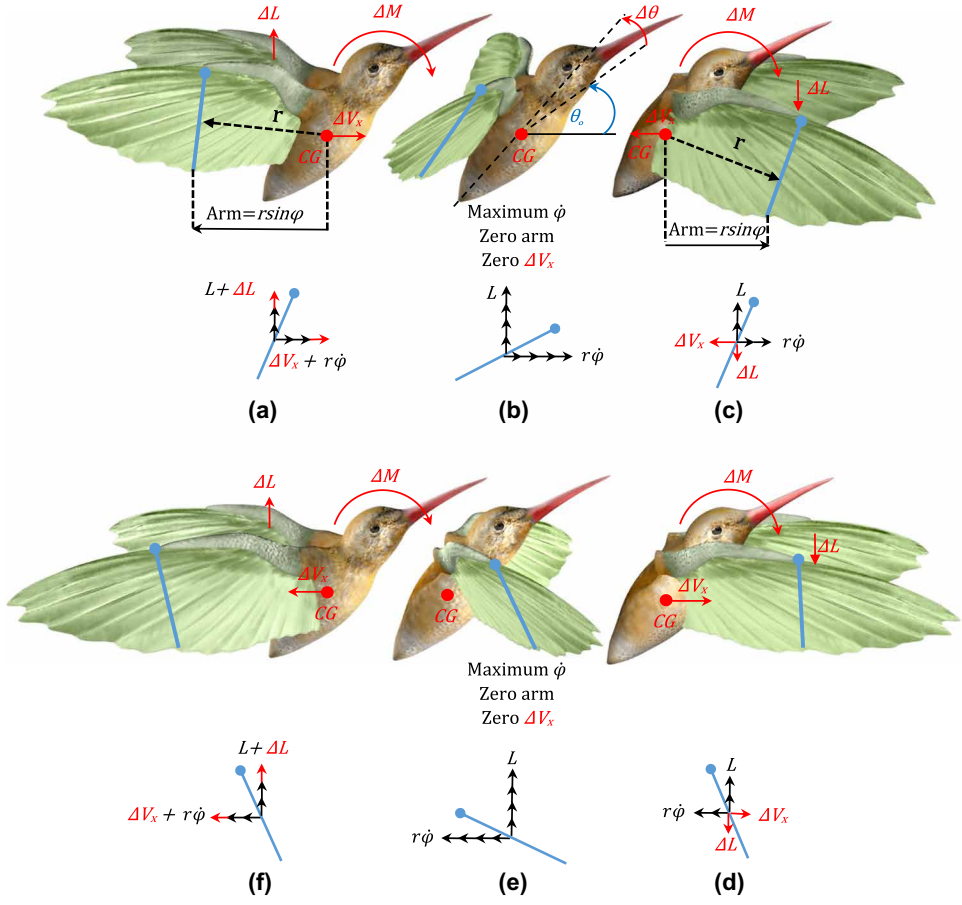

Fig. 4. Graphical illustration of the vibrational stabilization underlying physics. The figure shows a sequence of events over the first flapping cycle following a pitch up disturbance. Below each wing position, a wing section is shown with its speed relative to the surrounding quiescent air and the generated lift force. A pitch up disturbance Δθ [shown in (b)] causes a backward acceleration of the body $-g\sin\Delta\theta$. As such, the relative speed has two contributions: (i) the flapping speed that, for a wing section that is a distance r from the root, is given by $r\dot{\varphi}$, and (ii) the speed V_x induced by the body motion. Of particular interest to the vibrational stabilization mechanism is the oscillatory speed component ΔV_x of the body, which is due to oscillations in aerodynamic damping X_u, as explained above. The lift force due to flapping is L and the contribution of ΔV_x is ΔL; its associated pitching moment due to the oscillatory moment arm ($r\sin\varphi$) with respect to the body CG is ΔM. (**a**) Early position in downstroke: The body oscillatory speed ΔV_x is forward increasing the lift force, and the wing is behind the body CG resulting in a pitching down moment ΔM. (**b** and **e**) Middle position in downstroke/upstroke: The flapping speed is maximum, but the body oscillatory speed reaches zero along with the moment arm. (**c**) Late position in downstroke: The body oscillatory speed ΔV_x is backward decreasing the lift force, but the wing is ahead of the body CG, resulting in a pitching down moment ΔM too. (**d**) Early position in upstroke: The wing reverses its inclination and direction. The body oscillatory speed ΔV_x changes too; it becomes forward decreasing the lift force and resulting in a pitching down moment ΔM as the wing is still ahead of the body CG. (**f**) Late position in upstroke: The body oscillatory speed ΔV_x is backward (with the wing motion) increasing the lift force, but the wing is behind the body CG, resulting in a pitching down moment ΔM too. As a result, a net pitching down moment ΔM is generated over the flapping cycle that is proportional to the pitch disturbance—i.e., a restoring spring action.

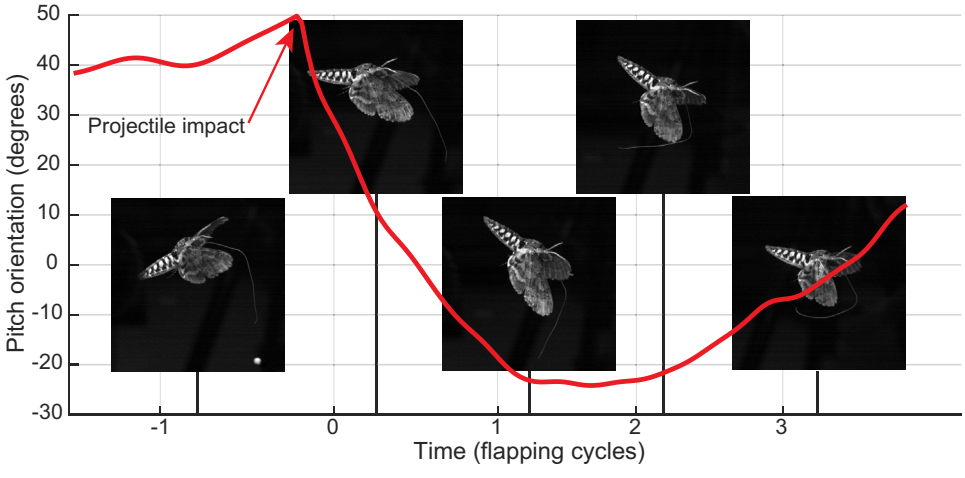

Fig. 5. In-flight perturbation of a hovering moth. The figure shows an image of the moth at the end of downstroke for five successive flapping cycles spanning the perturbation event and subsequent recover. The incoming projectile is visible in the leftmost video image; the perturbation impact occurs in the subsequent flapping cycle. The flapping cycles are not of exactly equal duration; the average flapping frequency for the cycles shown here was 28.8 Hz. Flapping cycle is numbered so as to begin and end at mid-downstroke. Last, the camera is positioned lateral and slightly above the moth, providing a view of both wingtips, although they are at the same elevation.

the vibrational contribution $\overline{\Delta M_{V_x}\Delta V_x}$ of the restoring pitching moment over the first cycle right after perturbation, as shown in Fig. 6E for the three cases. It was found that the averaged contribution is destabilizing, in agreement with several published results based on averaging (*9*, *10*, *13*, *46*). In contrast, the vibrational effects (due to the zero-mean oscillatory body motion and time-periodic dynamics) are stabilizing, which further supports the analysis and physical explanations presented in this work.

Performing a similar aerodynamic analysis on the hawkmoth experimental data, we also quantified the damping effects $M_q q$,

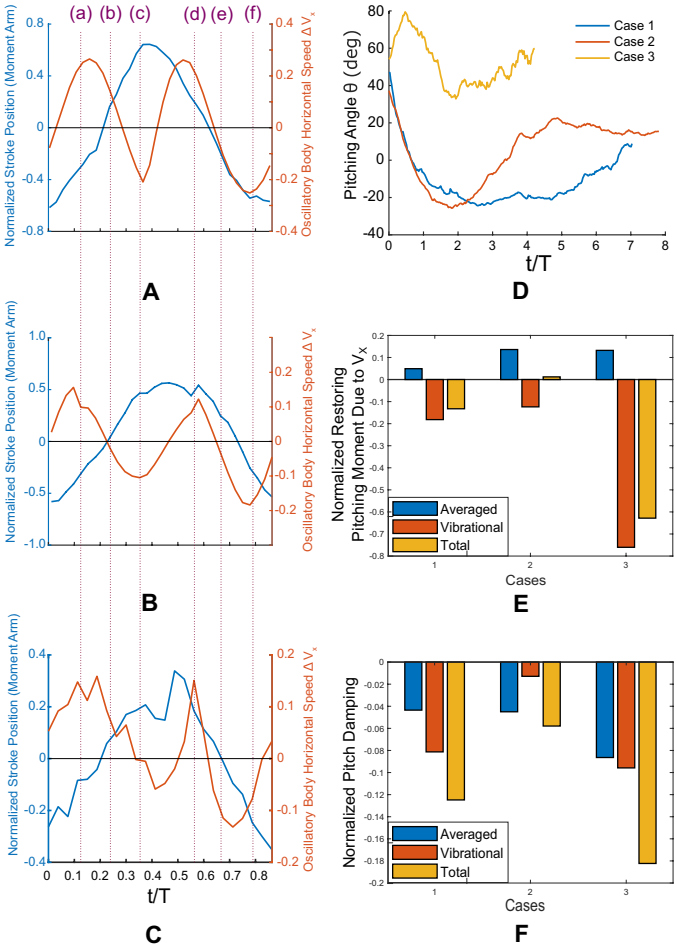

Fig. 6. Results of the hawkmoth perturbation experiment. (**A** to **C**) Synchronization between the response of the oscillatory component ΔV_x of the body horizontal speed and the stroke position represented by the moment arm from the wing tip to the body CG along the body axis. Three cases are considered: cases 1 and 2 are pitch down disturbance, and case 3 is pitch up. (a) Early position in downstroke: ΔV_x is positive, and the stroke position is negative (the wing is behind the body CG). (b and e) Middle position in downstroke/upstroke: Both ΔV_x and the stroke position cross zero. (c) Late position in downstroke: ΔV_x is negative and the stroke position is positive (the wing is ahead of the body CG). (d) Early position in upstroke: Both ΔV_x and the stroke position are positive. (f) Late position in upstroke: Both ΔV_x and the stroke position are negative. For the pitching down cases, $-\Delta V_x$ is plotted instead of ΔV_x for consistency of presentation. The plots are normalized: the body speed V_x by R/T and the stroke position by R. (**D**) Response of the body pitching angle θ in the three cases. (**E**) Comparison between the averaged contribution $\overline{M}_{V_x}\overline{V}_x$ and the vibrational contribution $\overline{\Delta M_{V_x}\Delta V_x}$ of the restoring pitching moment over the first cycle right after pitch disturbance in the three cases. The averaged contribution is destabilizing, whereas the vibrational contribution is stabilizing. (**F**) Similar analysis comparing the averaged pitch-damping contribution $\overline{M}_q\overline{q}$ with its vibrational contribution. The averaged pitch damping is stabilizing, which is augmented even more by its vibrational contribution. The restoring moments are normalized by the disturbance (initial pitch rate) and nondimensionalized by I_y/T^2.

decomposing it into averaged effects $\overline{M}_q\overline{q}$ and vibrational/oscillatory effects, as shown in Fig. 6F. The averaged pitch-damping effects are stabilizing, in accordance with the averaged model (Eq. 2) and the common knowledge in literature [flapping counter torque (*14*, *23*, *24*)]. Furthermore, the body's oscillations around the averaged motion induce a substantial additional (vibrational) pitch damping. That is, vibrational effects induce a notable pitch stiffness that is not captured at all by direct averaging and also considerably augment the averaged pitch damping.

The third case of the results shown in Fig. 6 (E and F) seems to refute the generally accepted notion that pitch-damping contributions are dominant: The contribution of pitch stiffness (due to V_x) in this third case is larger than that of pitch damping (due to q). To study this point in more detail, we performed several simulations of the nonlinear time-varying flight dynamic model (presented in the Supplementary Materials) due to different initial disturbances. In each simulation, we compared four contributions of the net recovering pitching moment over the first cycle after disturbance: the stiffness effect $M_{Vx}V_x$ identified in this paper, and the damping effect M_qq against their averaged contributions $\overline{M}_{V_x}\overline{V}_x$ and $\overline{M}_q\overline{q}$. Figure 7 shows such a comparison for two initial disturbances: (A) pitch disturbance of −5° and (B) pitch rate disturbance of −60°/s. The generally accepted concept of pitch-damping dominance is based on averaging, which is refuted in this paper: If we concern ourselves with the averaged contributions, then pitch-damping effects are always dominant, as shown in Fig. 7. However, if we consider the total effects (accounting for vibrational stabilization), then the early response over the first cycle really depends on the initial disturbance. For a given pitch disturbance $\theta_0 = -5^\circ$, the vibrational stiffness effects (due to V_x) are dominant, but for a pitch rate disturbance of $q_0 = -60^\circ/s$, the pitch-damping effects are dominant. This behavior is physically plausible: If the animal experiences a disturbance in the pitch angle (without disturbing the pitch rate), then the stiffness mechanism will be active at the beginning, whereas the damping mechanism will not be activated until later when the pitch rate is changed. Moreover, although the restoring pitching moments presented in Fig. 7 are normalized by the initial disturbance, the resulting sensitivities are not of the same order due to nonlinearity of the dynamics (sensitivity depends on the magnitude of the disturbance). In general, the combination of initial conditions (u_0, w_0, q_0, θ_0) would determine which mechanism is more dominant over the first cycle.

Scaling of vibrational stabilization in insect flight

Using chronological calculus, we applied second-order averaging to the time-varying dynamics (Eq. 1) and computed the eigenvalues of the linearization of this higher-order averaged dynamics around the hovering equilibrium for eight species that span a wide range of flapping frequencies and sizes—including the Harvard RoboFly micro air vehicle (MAV). Their morphological parameters are given in table S1, as taken from different sources (*14*, *47*–*51*). For simplicity, a horizontal stroke plane and a triangular flapping waveform are assumed (*52*, *53*).

Figure 8 shows a comparison of the real part (reciprocal of the time constant) of the most unstable eigenvalue, normalized by the flapping frequency, between the averaged dynamics (2) and the second-order averaged dynamics of the time-varying system (Eq. 1) for the eight species; the difference represents vibrational effects. Several facts can be inferred from Fig. 8: First, the averaged system (Eq. 2) is always unstable for all insects. Second, the vibrational effects are always stabilizing. Third, for large species with low flapping frequencies, such as the hummingbird and the hawkmoth, the stabilizing vibrational effects are strong enough to outweigh the instability of the averaged system (Eq. 2), resulting in a completely stable system—naturally without a need for feedback control. Fourth, as the flapping

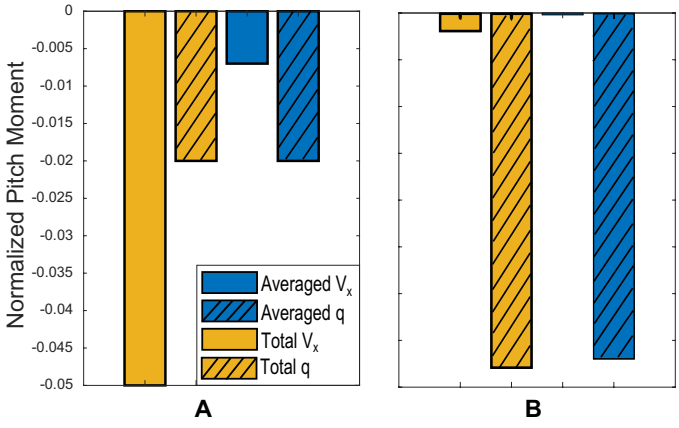

Fig. 7. On the dominance of pitch damping. Comparison for the restoring pitching moment over the first cycle between the indirect stiffness (due to V_x) and damping (due to q) for two different initial disturbances: (**A**) pitch disturbance −5° and (**B**) pitch rate disturbance −60°/*s*.

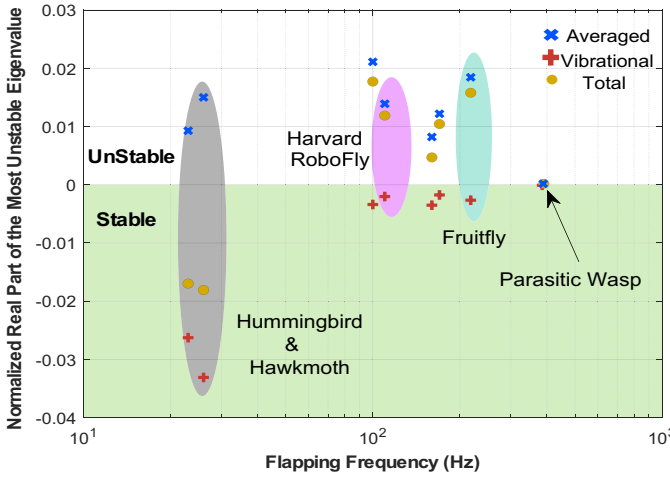

Fig. 8. Scaling of vibrational stabilization with animal's size and flapping frequency. The real part of the most unstable eigenvalue, normalized by the flapping frequency, of the averaged system (see Eq. 2) and the second-order averaged dynamics. The difference represents vibrational contributions.

frequency increases, the difference between direct averaging and second-order averaging is diminished [the main premise behind the averaging theory (*38*)]; for the tiny parasitic wasp flapping at 385 Hz (an order of magnitude higher than the hawkmoth), the eigenvalues of the two systems are almost identical. Therefore, for small insects flapping at high frequencies, direct averaging may be a valid analysis tool. Thus, these insects may need feedback control to stabilize their flight, which is concordant with the findings of Ristroph *et al.* (*46*), who discerned the feedback control mechanism used by fruit flies to stabilize their flight dynamics; fruit flies flap with too high frequency, at which vibrational stabilization is insufficient to provide passive stability as shown in Fig. 8, and hence, feedback control is needed.

The discovered vibrational effects are not expected to always fully stabilize large insects and flapping MAVs. We demonstrated full vibrational stabilization for one species of hawkmoth and hummingbird, but even in these animals, variation in morphological parameters may make them unstable even in the presence of vibrational stabilization. That being said, we should emphasize that the reported vibrational stabilization mechanism, even if insufficient in some cases, still provides a stabilizing action, which may help relax the required feedback control action and/or reduce complexity of the control architecture, making it more feasible for implementation with the limited resources offered with an insect's brain. These conclusions are particularly useful for MAVs. Engineers can tune the MAV parameters to strengthen the passive vibrational stabilization mechanism. It is noteworthy to mention several successful efforts that demonstrated stable hovering flight of flapping-wing MAVs, though using active flight control, such as the AeroVironment Nano Hummingbird (*54*), the Delft's Delfly (*55*), the Harvard RoboBee (*56*), the KU Beetle (*57*), the ULB Colibri (*58*), and the UCI Quad-Flapper (*59*).

DISCUSSION

The theoretical and experimental results presented in this paper call for a revision of some of the generally accepted concepts about flapping flight stability and instability. We show that direct averaging does not fully capture some essential dynamical features and stability characteristics, particularly for large flyers and flapping MAVs. The presented results imply that insects (and other high-frequency flapping flyers) experience vibrational stabilization, which contributes to the stability of the whole system. In other words, vibrational stabilization represents a passive mechanism that was not captured by earlier averaging-based modeling and analysis of insect flight. No matter how accurate a computational fluid dynamic (CFD) model is, if used to compute cycle-averaged stability derivatives, it cannot reveal the stabilizing oscillatory contributions revealed in this paper. These findings may lead to reassessment of some previous results. For example, Sane *et al.* (*60*) (Fig. 3) demonstrated that *M. sexta* antennae function as biological gyroscopes, enabling closed-loop stabilization. However, although *Manduca* without antennae fly less well than *Manduca* with antennae, they still fly, in sharp contrast to smaller insects such as fruit flies, which are unwilling or unable to take off if their gyroscopic sensor (the halteres) is disabled. The fact that *Manduca* can take off and fly in a small experimental enclosure after gross manipulation of their flight sensory system points to passive stability complemented by feedback control. That said, it remains possible that *Manduca* with amputated antennae may rely on other sensor modalities such as vision for feedback control. Further experiments that remove additional sensory inputs could better isolate the contribution of vibrational stability to overall flight control in *Manduca*.

The presented results of passive vibrational stabilization in flapping flight, particularly large insects, also smoothen a path toward evolution of flapping flight in that the oscillations required to flap the wings and produce lift also produce the required stability. Oscillatory locomotor mechanisms are ubiquitous in biology, and this result will spur research to check the exploitation of similar phenomena by animals with oscillatory cycles of limbs, fins, wings, or even cavities. It will also open the door for engineers to explore various designs of bioinspired flapping-wing MAVs where before the claimed instability hindered full exploration. Engineers can now relax the stability requirements by promoting vibrational stabilization in their designs and focus more on aerodynamic performance. It may be possible to design flapping-wing MAVs with simpler sensory control actuator processing systems, hence making miniaturization more feasible. The fact that the very instinctive flapping motion of the

wings—that is inevitably needed to produce the lift force keeping the insect aloft—naturally stabilize its flight dynamics without any feedback proposes a very intelligent design for future flapping-wing aerial robots.

MATERIALS AND METHODS

Flight dynamic modeling

Ignoring the wing structural and inertial effects, the equations of motion governing insect flight dynamics in the longitudinal plane are exactly the same as conventional aircraft, which are given in Eq. 7. They are written in an abstract form as

$$\dot{\boldsymbol{\chi}} = \mathbf{F}(\boldsymbol{\chi}, t) = \mathbf{f}(\boldsymbol{\chi}) + \mathbf{g}_a(\boldsymbol{\chi}, t) \tag{7}$$

where $\boldsymbol{\chi} = [u, w, q, \theta]$ is the state vector. The flight dynamic model used in this paper was developed in an earlier work (*17*). Here, we neglect higher-order dependence of the aerodynamic forces $\mathbf{g}_a$ on the state vector $\boldsymbol{\chi}$ and retain only the linear terms. As such, we write

$$\mathbf{g}_a(\boldsymbol{\chi}, t) = \mathbf{g}_0(t) + [\mathbf{G}(t)]\,\boldsymbol{\chi}$$

That is, we have

$$\begin{pmatrix} \dot{u} \\ \dot{w} \\ \dot{q} \\ \dot{\theta} \end{pmatrix} = \begin{pmatrix} -qw - g\sin\theta \\ qu + g\cos\theta \\ 0 \\ q \end{pmatrix} + \begin{pmatrix} X_0(t)/m \\ Z_0(t)/m \\ M_0(t)/I_y \\ 0 \end{pmatrix} + \begin{bmatrix} X_u(t) & X_w(t) & X_q(t) & 0 \\ Z_u(t) & Z_w(t) & Z_q(t) & 0 \\ M_u(t) & M_w(t) & M_q(t) & 0 \\ 0 & 0 & 0 & 0 \end{bmatrix} \begin{pmatrix} u \\ w \\ q \\ \theta \end{pmatrix} \tag{8}$$

Assuming a horizontal stroke plane, parameterized by the "back-and-forth" flapping angle φ and a piecewise constant variation in the wing pitch angle η, one obtains (*17*)

$$X_0(t) = -2K_{21}\dot{\varphi}(t)\,|\,\dot{\varphi}(t)\,|\cos\varphi(t)\sin^2\eta,$$
$$Z_0(t) = -K_{21}\dot{\varphi}(t)\,|\,\dot{\varphi}(t)\,|\sin 2\eta$$

$$M_0(t) = 2\dot{\varphi}(t)\,|\,\dot{\varphi}(t)\,|\sin\eta\,[K_{22}\Delta\hat{x}\cos\varphi(t) + K_{21}x_h\cos\eta(t) + K_{31}\sin j(t)\cos\eta]$$

where x_h is the distance from the vehicle center of mass to the root of the wing hinge line (i.e., the intersection of the hinge line with the x axis) and $\Delta\hat{x}$ is the chordwise distance from the center of pressure to this same hinge location, normalized by the chord length. Also, ρ is the air density, C_{L_α} is the 3D lift curve slope of the wing, $c(r)$ is the spanwise chord distribution, R is the wing radius, $I_{mn} = 2\int_0^R r^m c^n(r)\,dr$, and $K_{mn} = \frac{1}{4}\rho C_{L_\alpha} I_{mn}$. The time-varying stability derivatives are written directly in terms of the system parameters as (*17*)

$$X_u = -4\frac{K_{11}}{m}|\,\dot{\varphi}\,|\cos^2\varphi\sin^2\eta, \quad X_w = -\frac{K_{11}}{m}|\,\dot{\varphi}\,|\cos\varphi\sin 2\eta,$$
$$X_q = \frac{K_{21}}{m}\,|\,\dot{\varphi}\,|\sin\varphi\cos\varphi\sin 2\eta - x_h X_w$$

$$Z_u = 2X_w, \quad Z_w = -2\frac{K_{11}}{m}\,|\,\dot{\varphi}\,|\cos^2\eta, \quad Z_q = 2\frac{K_{21}}{m}\,|\,\dot{\varphi}\,|\,\sin\varphi\cos^2\eta - \frac{K_{\mathrm{rot}_{12}}}{m}\dot{\varphi}\cos\varphi - x_h Z_w$$

$$M_u = 4\frac{K_{12}\Delta\hat{x}}{I_y}\,|\,\dot{\varphi}\,|\cos^2\varphi\sin\eta + \frac{m}{I_y}(2X_q - x_h Z_u)$$

$$M_w = 2\frac{K_{12}\Delta\hat{x}}{I_y}|\,\dot{\varphi}\,|\cos\varphi\cos\eta + 2\frac{K_{21}}{I_y}|\,\dot{\varphi}\,|\sin\varphi\cos^2\eta - \frac{\mathrm{mx}_h}{I_y}\mathrm{Zw}$$

$$M_q = -\frac{2\Delta\hat{x}}{I_y}|\,\dot{\varphi}\,|\cos\varphi\cos\eta\left(K_{12}x_h + K_{22}\sin\varphi\right) + \frac{1}{I_y}\dot{\varphi}\cos\varphi\left(K_{\mathrm{rot}_{13}}\Delta\hat{x}\cos\varphi\cos\eta + K_{\mathrm{rot}_{22}}\sin\varphi\right) + -\frac{2}{I_y}|\,\dot{\varphi}\,|\cos^2\eta\sin\varphi\left(K_{21}x_h + K_{31}\sin\varphi\right) - \frac{K_v\mu_1 f}{I_y}\cos^2\varphi - \frac{\mathrm{mx}_h}{I_y}Z_q$$

where $K_{rot_{mn}} = \pi\rho\left(\frac{1}{2} - \Delta\hat{x}\right)I_{mn}$ and $K_v = \frac{\pi}{16}\rho I_{04}$. The hinge line is set at 30%c ($\Delta\hat{x} = 0.05$), x_h is assumed zero for simplicity, and the value of C_{L_α} is calculated based on the wing aspect ratio using the extended lifting theory according to Taha *et al.* (*61*). The above flight dynamic model has been developed in (*17*) and the resulting eigenvalues of the averaged, linearized dynamics have been validated against numerical simulations of Navier-Stokes equations by Sun *et al.* (*10*) and the experimental data of Cheng and Deng (*14*).

Derivation of Eq. 6

Because direct averaging of the dynamics (Eq. 8) does not reveal any pitch stiffness, the focus will be on the next term ($\boldsymbol{\Lambda}_2$) in the complete averaged dynamics (Eq. 5)

$$\boldsymbol{\Lambda}_2 = \frac{1}{2T}\int_0^T\left(\left[\frac{\partial\mathbf{F}(\boldsymbol{\chi},t)}{\partial\boldsymbol{\chi}}\right]\int_0^t\mathbf{F}(\boldsymbol{\chi},\tau)\,d\tau - \left[\frac{\partial\int_0^t\mathbf{F}(\boldsymbol{\chi},\tau)\,d\tau}{\partial\boldsymbol{\chi}}\right]\mathbf{F}(\boldsymbol{\chi},t)\right)dt$$

Its third component (i.e., the pitching dynamics) is written as

$$\boldsymbol{\Lambda}_2)_3 = \frac{1}{2T}\int_0^T(M_u(t)\,[(-qw - g\sin\theta)\,t + \widehat{X}_u(t)\,u + \widehat{X}_w(t)\,w + \widehat{X}_q(t)\,q] - \widehat{M}_u(t)\,[-qw - g\sin\theta + X_u(t)\,u + X_w(t)\,w + X_q(t)\,q] + M_w(t)\,[(qu - g(1-\cos\theta))\,t + \widehat{Z}_u(t)\,u + \widehat{Z}_w(t)\,w + \widehat{Z}_q(t)\,q] - \widehat{M}_w(t)\,[qu - g(1-\cos\theta) + Z_u(t)\,u + Z_w(t)\,w + Z_q(t)\,q] + M_q(t)\,[\widehat{M}_u u + \widehat{M}_w w + \widehat{M}_q q] - \widehat{M}_q\,[M_u(t)\,u + M_w w + M_q(t)\,q])\,dt$$

where the over hat indicates an integrated quantity, e.g., $\widehat{M}_u(t) = \int_0^t M_u(\tau)\,d\tau$. As such, the pitch stiffness is defined as $k_\theta = -\frac{\partial\boldsymbol{\Lambda}_2)_3}{\partial\theta}\,|\,_{\boldsymbol{\chi}=\boldsymbol{\chi}_0}$, where $\boldsymbol{\chi}_0 = [0,0,0,\theta_0]$ represents the hovering equilibrium point of the averaged dynamics. This definition yields

$$k_\theta = \frac{g}{2T}\int_0^T\left[\left(M_u(t)\,t - \int_0^t M_u(\tau)\,d\tau\right)\cos\theta_0 + \left(M_w(t)\,t - \int_0^t M_w(\tau)\,d\tau\right)\sin\theta_0\right]dt \tag{9}$$

where θ_0 is the averaged pitching angle at hover. Noting that

$$dM = [M_u \quad M_w]\begin{pmatrix} u \\ w \end{pmatrix} =$$
$$[M_u \quad M_w]\begin{bmatrix} \cos\theta_0 & -\sin\theta_0 \\ \sin\theta_0 & \cos\theta_0 \end{bmatrix}\begin{pmatrix} V_x \\ V_z \end{pmatrix} = [M_{V_x} \quad M_{V_z}]\begin{pmatrix} V_x \\ V_z \end{pmatrix}$$

we recognize $M_u\cos\theta_0 + M_w\sin\theta_0$ as M_{Vx} and, hence, arrive at Eq. 6 as

$$k_\theta = \frac{g}{2T}\int_0^T \left[M_{V_x}(t)\, t - \int_0^t M_{V_x}(\tau)\, d\tau \right] dt \qquad (10)$$

Processing of the moth experimental data

A 3D reconstruction of the high-speed videography (*62*) was performed to extract the time evolution of the position vector of each marker point (1 to 5), shown in fig. S1A, in an inertial frame. Points 1 to 3 were used to construct the body orientation with respect to the inertial frame, and points 3 to 5 were used to construct the wing orientation. Moreover, points 3 to 5 were used to determine the 2D translational velocity of each wing section and its pitching angular velocity. The inertial velocity vectors of points 3 to 5 (calculated via finite difference) are actually due to both (i) flapping motion of the wing and (ii) body motion. Therefore, subtracting them from the root (point 3) motion resulted in the wing flapping motion only, denoted by V_w. The motion of points 1 and 2 was used to determine the motion of the body CG, denoted by V_b. The horizontal component of this vector is denoted by V_x, which plays a key role in vibrational stabilization. This speed component was then decomposed into a slowly varying component $\overline{V}_x$ and a fast-oscillatory component ΔV_x: $V_x = \overline{V}_x + \Delta V_x$. We then fed the motion of each wing section (due to wing flapping motion only V_w) to the unsteady aerodynamic model below to determine an estimate for the stability derivative M_{V_x} over the cycle.

The adopted aerodynamic model is a refined version of our earlier model (*17*, *63*). Each wing is divided into 50 aerodynamic sections. For each section, the motion profile (e.g., due to V_w) of points 3 and 5 was used to determine the speed components V_{x_w} and V_{z_w} of the hinge point in the wing frame and the section pitching angular velocity ω_{y_w}, as shown in fig. S1B. Then, the aerodynamic forces and pitching moment in the wing frame are written as (*61*, *64*)

$$F_{x_w}(r,t) = -\rho\Gamma(r,t)\, V_{z_w}(r,t) - F_v(r,t)\, V_{x_w}(r,t),$$

$$F_{z_w}(r,t) = \rho\Gamma(r,t)\, V_{x_w}(r,t) - F_v(r,t)\, V_{z_w}(r,t) - m_a(r)\, a_{z_w}(r,t),$$

$$M_{y_w}(r,t) = (\rho\Gamma(r,t)\, V_{x_w}(r,t) - F_v(r,t)\, V_{z_w}(r,t))\, c(r)\, \Delta\hat{x} +$$

$$\frac{m_a(r)}{6} a_{z_w}(r,t)\, c(r) - \frac{\pi}{16}\rho c(r)^3 V_{x_w}(r,t)\, \omega_{y_w}(r,t) - \frac{\pi}{128}\rho c(r)^4 \dot{\omega}_{y_w}(r,t),$$

where the circulation Γ is given by

$$\Gamma(r,t) = -\frac{1}{4} c(r)\, C_{L_\alpha} \sin 2\alpha(r,t) \sqrt{V_{x_w}(r,t)^2 + V_{z_w}(r,t)^2} +$$

$$\pi c(r)^2 (1/2 - \Delta\hat{x})\, \omega_{y_w}(r,t)$$

and F_v represents the viscous friction drag: $F_v = \frac{1}{2}\rho\, c C_D \sqrt{V_{x_w}(r,t)^2 + V_{z_w}(r,t)^2}$, where C_D is the drag coefficient, which is given by $C_D = C_{D0}\cos^2\alpha + C_{D\pi/2}\sin^2\alpha$ with $C_{D0} = 0.07$, $C_{D\pi/2} = 3.06$ (*64*), and $\alpha = \tan^{-1}\frac{V_{z_w}}{V_{x_w}}$. Also, the added mass is given by $m_a = \frac{\pi}{4}\rho c^2$, and a_{zw} is the acceleration of the mid-chord point in the z_w axis.

The aerodynamic forces F_{x_w} and F_{z_w} were transformed into the inertial frame and integrated over the wing span to obtain the total lift force. The ratio of the averaged lift before perturbation to the insect weight was found to be 1 ± 0.1 for all of the three considered cases, which gives some confidence in the adopted aerodynamic model. Also, these forces are multiplied by the arm from the hinge location at each section to the body CG to obtain the moment vector. Adding it to the component M_{y_w}, transforming the result into the body frame, and integrating over the cycle, we obtained the total pitching moment $M_{y_{CG}}$ and then normalized it by $I_y T^2$.

The complex-step finite difference was used to obtain accurate approximation for the stability derivative M_{Vx}. The aerodynamic model described above was run with velocities due to the wing flapping motion V_w and an infinitesimal perturbation in the body horizontal speed V_x in the imaginary direction (i.e., in the complex plane): $V_w + i\delta V_x$, where δ is a small number representing the infinitesimal change. The advantage of the complex step finite difference approach mainly lies in the fact that its accuracy in approximating derivatives increases monotonically with decreasing the step size. That is, in contrast to the traditional finite difference, it does not suffer from a roundoff error when decreasing the step size beyond a certain limit. Therefore, we used the machine precision value for δ to get the best estimate for the derivative M_{Vx} as

$$M_{V_x} = \frac{1}{I_y}\frac{\partial M}{\partial V_x}, \quad \frac{\partial M}{\partial V_x} = \frac{\mathrm{imag}(M_{y_{CG}}(V_w + i\delta V_x))}{\delta}$$

Morphological parameters

The following morphological parameters were needed for each insect/MAV to perform the analysis presented in this paper: the body mass m and pitching moment of inertia I_y, the flapping amplitude Φ and frequency n, the wing length R, and the wing chord distribution $c(r)$. As for this last item, whenever enough data are available about the wing geometry, the method of moments used by Ellington (*48*) is adopted as follows. Given the wing length R, mean chord length $\bar{c}$, and first two moments of area $\hat{r}_1$ and $\hat{r}_2$, which are defined as $I_{k1} = 2\int_0^R r^k c(r)\, dr = 2\mathrm{S}\mathrm{R}^k \hat{r}_k^k$, where $S = R\bar{c}$ and the wing chord distribution is written as (*48*)

$$c(r) = \frac{\bar{c}}{\beta}\left(\frac{r}{R}\right)^{\upsilon-1}\left(1 - \frac{r}{R}\right)^{\gamma-1} \qquad (11)$$

where

$$\upsilon = \hat{r}_1\left[\frac{\hat{r}_1(1-\hat{r}_1)}{\hat{r}_2^2 - \hat{r}_1^2} - 1\right], \gamma = (1-\hat{r}_1)\left[\frac{\hat{r}_1(1-\hat{r}_1)}{\hat{r}_2^2 - \hat{r}_1^2} - 1\right], \text{and}$$

$$\beta = \int_0^1 \hat{r}^{\upsilon-1}(-\hat{r})^{\gamma-1} d\hat{r}$$

If the two moments $\hat{r}_1$ and $\hat{r}_2$ of the wing chord distribution are not available, an elliptic chord distribution is assumed

$$c(r) = \frac{4\bar{c}}{\pi}\sqrt{1 - r^2/R^2} \qquad (12)$$

For some other insects such as the parasitic wasp, a triangular chord distribution is adopted according to Weis-Fogh (*47*)

$$c(r) = 2\bar{c}\frac{r}{R} \qquad (13)$$

Table S1 presents the morphological parameters needed to conduct the analysis of this paper.

SUPPLEMENTARY MATERIALS

robotics.sciencemag.org/cgi/content/full/5/46/eabb1502/DC1

Fig. S1. A schematic diagram for postprocessing of the hawkmoth experiment.

Table S1. Operating conditions and morphological parameters for the species/MAVs considered in this work.

Movie S1. The experiment on the hawkmoth.

Movie S2. Our demonstration of vibrational stabilization on a robotic flapper.

Movie S3. The vibrational stabilization phenomenon on the inverted pendulum and how it induces a spring action.

Movie S4. The unstable response of the propeller setup due to the lack of vibration (oscillation).

REFERENCES AND NOTES

1. R. Å. Norberg, *Swimming and Flying in Nature* (Springer, 1975), pp. 763–781.
2. R. Dudley, C. P. Ellington, Mechanics of forward flight in bumblebees: II. Quasi-steady lift and power requirements. *J. Exp. Biol.* **148**, 53–88 (1990).
3. C. P. Ellington, in *Biological Fluid Dynamics*, C. P. Ellington, T. J. Pedley, Eds. (The Society for Experimental Biology, 1995), vol. 49, pp. 109–129.
4. A. P. Willmott, C. P. Ellington, The mechanics of flight in the hawkmoth Manduca sexta. II. Aerodynamic consequences of kinematic and morphological variation. *J. Exp. Biol.* **200**, 2723–2745 (1997).
5. C. P. Ellington, C. van den Berg, A. P. Willmott, A. L. R. Thomas, Leading-edge vortices in insect flight. *Nature* **384**, 626–630 (1996).
6. M. H. Dickinson, F.-O. Lehmann, S. P. Sane, Wing rotation and the aerodynamic basis of insect flight. *Science* **284**, 1954–1960 (1999).
7. G. K. Taylor, A. L. R. Thomas, Animal flight dynamics II. Longitudinal stability in flapping flight. *J. Theor. Biol.* **214**, 351–370 (2002).
8. G. K. Taylor, A. L. R. Thomas, Dynamic flight stability in the desert locust *Schistocerca gregaria*. *J. Theor. Biol.* **206**, 2803–2829 (2003).
9. M. Sun, Y. Xiong, Dynamic flight stability of a hovering bumblebee. *J. Exp. Biol.* **208**, 447–459 (2005).
10. M. Sun, J. Wang, Y. Xiong, Dynamic flight stability of hovering insects. *Acta Mech. Sin.* **23**, 231–246 (2007).
11. Y. Xiong, M. Sun, Dynamic flight stability of a bumblebee in forward flight. *Acta Mech. Sin.* **24**, 25–36 (2008).
12. N. Gao, H. Aono, H. Liu, A numerical analysis of dynamic flight stability of hawkmoth hovering. *J. Biomech. Sci. Eng.* **4**, 105–116 (2009).
13. I. Faruque, J. S. Humbert, Dipteran insect flight dynamics. Part. 1. Longitudinal motion about hover. *J. Theoret. Biol.* **264**, 538–552 (2010).
14. B. Cheng, X. Deng, Translational and rotational damping of flapping flight and its dynamics and stability at hovering. *IEEE Trans. Robot.* **27**, 849–864 (2011).
15. L. Schenato, "Analysis and control of flapping flight: From biological to robotic insects," thesis, University of Califorina Berkeley (2003).
16. R. C. Nelson, *Flight Stability and Automatic Control* (WCB/McGraw Hill, 1998), vol. 2.
17. H. Taha, M. R. Hajj, A. H. Nayfeh, Longitudinal flight dynamics of hovering MAVs/Insects. *J. Guid. Control Dyn.* **37**, 970–979 (2014).
18. G. K. Taylor, R. Zbikowski, Nonlinear time-periodic models of the longitudinal flight dynamics of desert locusts Schistocerca gregaria. *J. R. Soc. Interface* **1**, 197–221 (2005).
19. N. Gao, H. Liu, Passive dynamic stability of a hovering fruit fly: A comparison between linear and nonlinear methods. *J. Biomech. Sci. Eng.* **5**, 591–602 (2010).
20. C. T. Orlowski, A. R. Girard, Modeling and simulation of nonlinear dynamics of flapping wing micro air vehicles. *AIAA J.* **49**, 969–981 (2011).
21. C. T. Orlowski, A. R. Girard, Averaging of the nonlinear dynamics of flapping wing micro air vehicles for symmetrical flapping (AIAA, 2011); https://arc.aiaa.org/doi/abs/10.2514/6.2011-1228.
22. A. Banazadeh, N. Taymourtash, Adaptive attitude and position control of an insect-like flapping wing air vehicle. *Nonlinear Dyn.* **85**, 47–66 (2016).
23. T. L. Hedrick, B. Cheng, X. Deng, Wingbeat time and the scaling of passive rotational damping in flapping flight. *Science* **324**, 252–255 (2009).
24. B. Cheng, S. Fry, Q. Huang, X. Deng, Aerodynamic damping during rapid flight maneuvers in the fruit fly Drosophila. *J. Exp. Biol.* **213**, 602–612 (2010).
25. L. Ristroph, A. J. Bergou, G. Ristroph, K. Coumes, G. J. Berman, J. Guckenheimer, Z. J. Wang, I. Cohen, Discovering the flight autostabilizer of fruit flies by inducing aerial stumbles. *Proc. Natl. Acad. Sci. U.S.A.* **107**, 4820–4824 (2010).
26. B. Cheng, X. Deng, T. L. Hedrick, The mechanics and control of pitching manoeuvres in a freely flying hawkmoth (*Manduca sexta*). *J. Exp. Biol.* **214**, 4092–4106 (2011).
27. S.-Y. Choi, J.-K. Kim, J.-s. Han, J.-H. Han, *SPIE Smart Structures and Materials+ Nondestructive Evaluation and Health Monitoring* (International Society for Optics and Photonics, 2015), pp. 94291K.
28. N. J. Strausfeld, *Atlas of an Insect Brain* (Springer Science & Business Media, 2012).
29. R. Zbikowski, Aerodynamics: Red admiral agility. *Nature* **420**, 615–617 (2002).
30. M. H. Dickinson, Haltere–mediated equilibrium reflexes of the fruit fly, Drosophila melanogaster. *Philos. Trans. R. Soc. Lond. B Biol. Sci.* **354**, 903–916 (1999).
31. B. H. Dickerson, Z. N. Aldworth, T. L. Daniel, Control of moth flight posture is mediated by wing mechanosensory. *J. Exp. Biol.* **2014217**, 2301–2308 (2014).
32. H. K. Khalil, *Noninear Systems* (Prentice-Hall, 2002).
33. J. M. Berg, I. M. Wickramasinghe, Vibrational control without averaging. *Automatica* **58**, 72–81 (2015).
34. J. A. Sanders, F. Verhulst, J. A. Murdock, *Averaging Methods in Nonlinear Dynamical Systems* (Springer, 2007), vol. 2.
35. A. A. Agrachev, R. V. Gamkrelidze, Exponential representation of flows and a chronological enumeration. *Mat. Sb.* **107**, 467–532 (1978).
36. A. Sarychev, Stability criteria for time-periodic systems via high-order averaging techniques, in *Nonlinear Control in the Year 2000*, A. Isidori, F. Lamnabhi-Lagarrigue, W. Respondek, Eds., vol. 2 of *Lecture Notes in Control and Information Sciences* (Springer-Verlag, 2001), pp. 365–377.
37. P. A. Vela, "Averaging and control of nonlinear systems (with application to biomimetic locomotion)," thesis, California Institute of Technology, Pasadena, CA (2003).
38. M. Maggia, S. Eisa, H. Taha, On higher-order averaging of time-periodic systems: Reconciliation of two averaging techniques. *Nonlinear Dyn.* **99**, 813–836 (2020).
39. J. Baillieul, B. Lehman, Open-loop control using oscillatory inputs, in *The Control Systems Handbook* (CRC Press, 1996), pp. 967–980.
40. F. Bullo, Averaging and vibrational control of mechanical systems. *SIAM J. Control Optim.* **41**, 542–562 (2002).
41. A. H. Nayfeh, D. T. Mook, *Nonlinear Oscillations* (John Wiley and Sons Inc., 1979).
42. A. Stephenson, XX. On induced stability. *London, Edinburgh, Dublin Philos. Mag. J. Sci.* **15**, 233–236 (1908).
43. P. L. Kapitza, Pendulum with vibrating suspension. *Uspekhi Fiz. Nauk* **44**, 7–20 (1951).
44. P. L. Kapitza, Dynamical stability of a pendulum when its point of suspension vibrates, in *Collected Papers by P.L. Kapitza* (Pergamon, 1965), vol. 2, pp. 714–726.
45. Stabilization of an inverted pendulum under high-frequency excitation (kapitza pendulum); https://www.youtube.com/watch?v=GgYABmG_bto [accessed 25 October 2016].
46. L. Ristroph, G. Ristroph, S. Morozova, A. J. Bergou, S. Chang, J. Guckenheimer, Z. J. Wang, I. Cohen, Active and passive stabilization of body pitch in insect flight. *J. R. Soc. Interface* **10**, 20130237 (2013).
47. T. Weis-Fogh, Quick estimates of flight fitness in hovering animals, including novel mechanisms for lift production. *J. Exp. Biol.* **59**, 169–230 (1973).
48. C. P. Ellington, The aerodynamics of hovering insect flight. II. Morphological parameters. *Philos. Trans. R. Soc. Lond. B* **305**, 17 (1984).
49. A. R. Ennos, Inertial and aerodynamic torques on the wings of diptera in flight. *J. Exp. Biol.* **142**, 87–95 (1989).
50. P. Chai, D. Millard, Flight and size constraints: Hovering performance of large hummingbirds under maximal loading. *J. Exp. Biol.* **200**, 2757–2763 (1997).
51. D. B. Doman, M. W. Oppenheimer, D. O. Sigthorsson, Wingbeat shape modulation for flapping-wing micro-air-vehicle control during hover. *J. Guid. Control Dynam.* **33**, 724–739 (2010).
52. C. P. Ellington, The aerodynamics of hovering insect flight. III. Kinematics. *Philos. Trans. R. Soc. Lond. B* **305**, 41–78 (1984).
53. J. M. Zanker, The wing beat of *Drosophila Melanogaster*. III. Control. *Philos. Trans. R. Soc. Lond. B Biol. Sci.* **327**, 45–64 (1990).
54. M. Keennon, K. Klingebiel, H. Won, Development of the nano hummingbird: A tailles flapping wing micro air vehicle (AIAA, 2012); https://arc.aiaa.org/doi/10.2514/6.2012-588.
55. G. C. H. E. De Croon, M. A. Groen, C. De Wagter, B. Remes, R. Ruijsink, B. W. van Oudheusden, Design, aerodynamics and autonomy of the DelFly. *Bioinspir. Biomim.* **7**, 025003 (2012).
56. R. Wood, R. Nagpal, G.-Y. Wei, Flight of the robobees. *Sci. Am.* **308**, 60–65 (2013).
57. H. V. Phan, T. Kang, H. C. Park, Design and stable flight of a 21 g insect-like tailless flapping wing micro air vehicle with angular rates feedback control. *Bioinspir. Biomim.* **12**, 036006 (2017).
58. A. Roshanbin, H. Altartouri, M. Karásek, A. Preumont, COLIBRI: A hovering flapping twin-wing robot. *Int. J. Micro Air Veh.* **9**, 270–282 (2017).
59. M. Kiani, B. Davis, F. P. Quevedo, N. Cabezut, S. Hince, M. Balta, H. Taha, A new bioinspired flying concept: The Quadflapper (AIAA, 2019); https://arc.aiaa.org/doi/10.2514/6.2019-1048.
60. S. P. Sane, A. Dieudonné, M. A. Willis, T. L. Daniel, Antennal mechanosensors mediate flight control in moths. *Science* **315**, 863–866 (2007).
61. H. Taha, M. R. Hajj, P. S. Beran, State-space representation of the unsteady aerodynamics of flapping flight. *Aerosp. Sci. Technol.* **34**, 1–11 (2014).
62. T. L. Hedrick, Software techniques for two- and three-dimensional kinematic measurements of biological and biomimetic systems. *Bioinspir. Biomim.* **3**, 034001 (2008).
63. H. Taha, A. H. Nayfeh, M. R. Hajj, Aerodynamic-dynamic interaction and longitudinal stability of hovering MAVs/insects, AIAA 2013-1707.

64. G. J. Berman, Z. J. Wang, Energy-minimizing kinematics in hovering insect flight. *J. Fluid Mech.* **582**, 153–168 (2007).

Acknowledgments: H.E.T. acknowledges the fruitful discussions with Y. Aboelkassem, M. Fouda, G. Berman, and A. Roman. M.K. and H.E.T. are very grateful to the help of J. Navarro during his internship at UC Irvine on the robotic flapper demonstration and the efforts of Z. Montazeri for her help editing Fig. 4. Finally, H.E.T. would like to dedicate this effort in the memory of Prof. Ali Nayfeh—the man who never accepted direct averaging for the analysis of flapping flight. **Funding:** This project was supported by National Science Foundation grant CMMI-1846308 and the Air Force Office of Scientific Research under award number FA9550-19-1-0126, monitored by G. Abate, to H.E.T.; NSF IOS-0920358 and IOS-1253276 to T.L.H.; and NDSEG Fellowship to J.S.M.G. **Author contributions:** H.T. performed theoretical flight dynamics analysis and aerodynamic postprocessing of the hawkmoth experiment. M.K. developed a robotic flapper demonstration. T.L.H. developed the Hawkmoth experiment and the kinematic postprocessing. J.S.M.G. performed this experiment. Last, H.E.T. and T.L.H. wrote the paper. **Competing interests:** J.S.M.G. is an inventor on a provisional patent, "Methods for maximizing stability in flapping micro air vehicles." The other authors declare that they have no known competing financial interests or personal relationships that could have appeared to influence the work reported in this paper. **Data and materials availability:** All data needed to evaluate the conclusions in the paper are present in the paper or the Supplementary Materials, and the Hawkmoth data used for this study have been deposited in the database https://figshare.com/s/91548713290e58c43a9f.

Submitted 3 February 2020
Accepted 8 September 2020
Published 30 September 2020
10.1126/scirobotics.abb1502

Citation: H. E. Taha, M. Kiani, T. L. Hedrick, J. S. M. Greeter, Vibrational control: A hidden stabilization mechanism in insect flight. *Sci Robot.* **5**, eabb1502 (2020).

Science Robotics

Vibrational control: A hidden stabilization mechanism in insect flight

Haithem E. Taha, Mohammadali Kiani, Tyson L. Hedrick, and Jeremy S. M. Greeter

Sci. Robot. **5** (46), eabb1502. DOI: 10.1126/scirobotics.abb1502

Science Robotics (ISSN 2470-9476) is published by the American Association for the Advancement of Science. 1200 New York Avenue NW, Washington, DC 20005. The title *Science Robotics* is a registered trademark of AAAS.